Applied Catalysis B: Environmental 142–143 (2013) 414–422

Contents lists available at SciVerse ScienceDirect

Applied Catalysis B: Environmental

journal homepage: www.elsevier.com/locate/apcatb

In situ synthesis of cobalt–phosphate (Co–Pi) modified g-C_3N_4 photocatalysts with enhanced photocatalytic activities

Lei Ge[a,b,*], Changcun Han[a], Xinlai Xiao[b], Lele Guo[b]

[a] State Key Laboratory of Heavy Oil Processing, College of Sciences, China University of Petroleum Beijing, No. 18 Fuxue Road, Beijing 102249, People's Republic of China

[b] Department of Materials Science and Engineering, College of Sciences, China University of Petroleum Beijing, No. 18 Fuxue Road, Beijing 102249, People's Republic of China

ARTICLE INFO

Article history:
Received 28 January 2013
Received in revised form 26 April 2013
Accepted 22 May 2013
Available online 30 May 2013

Keywords:
Cobalt–phosphate (Co–Pi)
Graphitic carbon nitride
Water splitting
Photocatalysis

ABSTRACT

The novel cobalt–phosphate (Co–Pi) modified graphitic carbon nitride (g-C_3N_4) photocatalysts were synthesized by "in situ" surface photodeposition process to enhance photocatalytic H_2 and O_2 evolution performance. The resulting Co–Pi/g-C_3N_4 composite photocatalysts were characterized by X-ray diffraction (XRD), scanning electron microscopy (SEM), X-ray photoelectron spectroscopy (XPS) and photoluminescence spectroscopy (PL). The photoelectrochemical measurements of the composite materials were also performed under visible light irradiation. In the photodeposition process, the photogenerated holes in the valence band can oxidize Co^{2+} ions into Co^{3+} ions and cause the deposition of Co–Pi catalysts on the g-C_3N_4 surface. The photocatalytic results indicate that the Co–Pi catalysts can promote the separation of photogenerated charge carriers in g-C_3N_4 and enhance H_2 and O_2 evolutions. One of the synthesized samples CP-20 exhibits the highest catalytic activity. The corresponding O_2 and H_2 evolutions of the CP-20 are 6.8 and 9.6 times than the photocatalytic activities of unmodified g-C_3N_4. A possible mechanism on the improvement of visible light performance is proposed; and this can pave the way for the design and synthesis of new photocatalytic materials.

1. Introduction

The solar energy driven water splitting and pollutants degradation through semiconductor photocatalysis is of great importance as it is a promising technique for renewable energy production and environmental purification [1–6]. Efficient photocatalytic process requires both a highly active semiconductor catalyst and good working stability, especially for water splitting reaction [7–11]. Many visible light photocatalysts have been designed and explored in order to efficiently utilize solar energy [12–18]. In spite of great research efforts in recent decades for visible-light-driven photocatalysts [19–23], the number of semiconductors with high photocatalytic efficiency and stability under visible light illumination is still limited [24]. Therefore, developing new and more efficient visible light photocatalysts has become crucial to meet the requirements of future solar energy technologies.

As the most stable phase of carbon nitride compounds under ambient conditions, polymeric graphitic carbon nitride (g-C_3N_4) has received much attention as a promising "metal-free" photocatalyst working under visible light [25]. g-C_3N_4 has an ideal bandgap (E_g) of approximately 2.7 eV [25,26], which allows for utilizing a significant visible portion of the solar spectrum [27,28]. Its conduction band and valence band positions have sufficient overpotential for H_2 and O_2 evolution [29]. Furthermore, g-C_3N_4 is composed of inexpensive "earth abundant" elements, and can be synthesized by facile synthetic methods [30,31]. However, for use as an efficient photocatalyst for water splitting, g-C_3N_4 suffers from low separation efficiency of photogenerated electron–hole pairs [32]. Many strategies have been developed to overcome these challenges, which include the synthesis of novel nanostructures [33,34], tuning compositions [35–38], construction of heterojunctions [39–41] and sensitizing the materials by organic dyes [42]. Recently, Zhang et al. [29] reported the Co_3O_4/g-C_3N_4 hybrid photocatalytsts with enhanced O_2 evolution activity, indicating that Co-based species can be used to improve the photocatalytic activity in the C_3N_4 based materials.

Recently, earth abundant cobalt phosphate (Co–Pi) has been demonstrated to work effectively as oxygen-evolving electrocatalyst [43–45]. This material has attractive characteristics such as the low cost and self-repairing behavior [46,47]. The Co–Pi species has been effectively integrated with semiconductors such as ZnO [44], WO_3 [48], α-Fe_2O_3 [49], Si [50] and $BiVO_4$ [51,52], in order to

* Corresponding author at: Department of Materials Science and Engineering, College of Sciences, China University of Petroleum Beijing, No. 18 Fuxue Road, Beijing 102249, People's Republic of China. Tel.: +86 1089739096.
E-mail address: gelei08@163.com (L. Ge).

0926-3373/$ – see front matter © 2013 Elsevier B.V. All rights reserved.
http://dx.doi.org/10.1016/j.apcatb.2013.05.051

enhance the performance of photocatalytic efficiency. So far, most of the reports have focused on the improved photocurrent in photoelectrochemical water oxidation for O_2 evolution. Very recently, Wang et al. [53] prepared Co–Pi/$BiVO_4$ photocatalysts via photodeposition process, and found that the O_2 evolution can be enhanced to 6.8 times on the composite catalysts. Xu et al. [54] synthesized Co–Pi/ZnO hybrid photocatalysts, the enhanced activity for O_2 evolution was observed in water oxidation, and the O_2 evolution was more than 4 times of that obtained from pure ZnO. Therefore, it is desirable to deposit Co–Pi on alternative photocatalysts and to further understand the synergistic effect of Co–Pi and other materials.

In this work, for the first time, the novel Co–Pi/g-C_3N_4 composite photocatalysts were synthesized via a facile "in situ" photodeposition method. The photocatalytic O_2 and H_2 evolution via water splitting were investigated under visible light irradiation to evaluate the catalytic performance of composite samples. The Co–Pi modified g-C_3N_4 exhibited significantly enhanced photocatalytic activity, and the g-C_3N_4 with deposition time of 20 min (CP-20) showed the highest performance. The corresponding O_2 and H_2 evolution activities were 6.8 and 9.6 times higher than that of pure g-C_3N_4. The effects of increased light absorption, efficient charge transfer and separation on the photocatalytic performance were discussed in detail. A possible photocatalytic mechanism was proposed based on the experimental results. This study provides a facile way to synthesize photocatalysts made of earth abundant elements for potential high-efficiency photocatalytic applications.

2. Experimental

2.1. Synthesis of the photocatalysts

All chemicals were reagent grade and used without further purification. The metal-free g-C_3N_4 powders were synthesized by heating 2.0 g of cyanamide in an alumina combustion boat under nitrogen gas flow (10 ml/min) to 550 °C at a heating rate of 10 °C min^{-1} followed by 4 h at that temperature prior to cooling. The product was collected and ground into a powder.

"In situ" synthesis of Co–Pi/g-C_3N_4 composite photocatalysts was described as follows: 0.4 g g-C_3N_4 was immersed in a glass beaker with 100 ml aqueous buffer solution (pH = 7) containing 0.1 M potassium phosphate and 0.5 mM cobalt nitrate hexahydrate ($Co(NO_3)_2{\cdot}6H_2O$). Photodepositions were performed using a PLS-SXE 300UV Xe arc lamp as UV light source. The mixed g-C_3N_4 and buffer solution were mechanically stirred for several minutes under UV light irradiation. After photodepositions, samples were rinsed thoroughly with distill water and dried in vacuum environment. The UV irradiation time of Co–Pi/g-C_3N_4 composite samples were 5, 10, 20, 30, 60 min; the resulting samples were denoted as CP-5, CP-10, CP-20, CP-30 and CP-60, respectively.

2.2. Characterization

The crystal structure of the samples was investigated using X-ray diffraction (XRD; Bruker D8 Advance X-ray diffractometer) with Cu Kα radiation at a scan rate of 0.1° $2\theta\ s^{-1}$. The accelerating voltage and the applied current were 40 kV and 40 mA, respectively. The morphology of the samples was examined by field emission scanning electron microscopy (SEM; FEI Quanta 200F; accelerating voltage = 10 kV). X-ray photoelectron spectroscopy (XPS) measurements were done on a Axis Ultra XPS instrument with an Mg Kα source. The photoluminescence (PL) spectra of the photocatalyst were obtained by a Varian Cary Eclipse spectrometer with excitation wavelength of 325 nm.

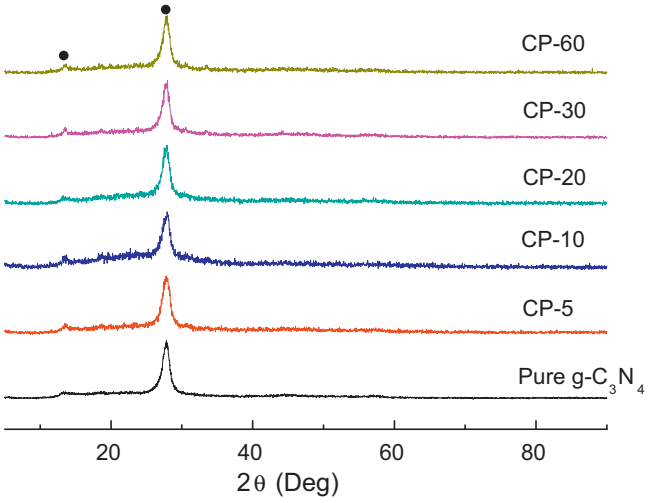

Fig. 1. XRD patterns of pure g-C_3N_4 and the Co–Pi/g-C_3N_4 composite photocatalysts.

2.3. Photocatalytic activity

The photocatalytic H_2 evolution experiments were performed in a 300 ml quartz reactor at ambient temperature. The reactor is connected to a closed circulating system. As light source, a PLS-SXE 300UV Xe arc lamp with a UV-cutoff filter (>400 nm) was used. In a typical photocatalytic experiment, 0.1 g of photocatalyst powder was suspended in 120 ml of aqueous solution containing 25% methanol by volume. The loading of 1.0 wt% Pt co-catalyst was conducted by directly dissolving H_2PtCl_6 into the mentioned suspension. Next, the suspensions were stirred and irradiated (300 W Xe arc lamp) for 30 min at room temperature to reduce the Pt species. Before photocatalytic experiments, the reaction vessel was evacuated for 30 min to remove the dissolved oxygen and to ensure the anaerobic conditions. The products were analyzed by gas chromatography (Shimadzu GC-8A, high purity Argon as a carrier gas) equipped a thermal conductivity detector. The photocatalytic O_2 evolution experiments were similar to the H_2 evolution: 0.1 g of photocatalyst powder was dispersed in 120 ml of 0.05 M silver nitrate ($AgNO_3$) solution. The suspensions were evacuated for at least 30 min before irradiation to remove dissolved air. Then it was irradiated for 3 h using the 300 W Xe arc lamp with a UV-cutoff filter (>400 nm), and the O_2 evolution were detected by gas chromatography (Shimadzu GC-8A).

2.4. Photoelectrochemical measurements

Photocurrent measurements were performed on an electrochemical analyzer (Solartron SI 1287 Instruments) in a standard three-electrode configuration with a Pt wire as the counter electrode, and Ag/AgCl (in saturated KCl) as a reference electrode. Irradiation proceeded by a Xe arc lamp through a UV-cutoff filter (λ > 420 nm). Na_2SO_4 (0.01 M) aqueous solution was used as the electrolyte. The working electrodes were prepared as follows: the 0.05 g ground sample was mixed with 1 ml distilled water and 0.1 ml Liquion solution (Ion Power Inc.) was added to make slurry. The slurry was then injected onto a 2 cm × 0.5 cm FTO glass electrode and these electrolytes were dried at 120 °C for 30 min.

3. Results and discussion

3.1. Characterization of Co–Pi/g-C_3N_4 composite samples

The X-ray diffraction patterns of as-prepared Co–Pi/g-C_3N_4 photocatalysts are shown in Fig. 1. The pure polymeric g-C_3N_4

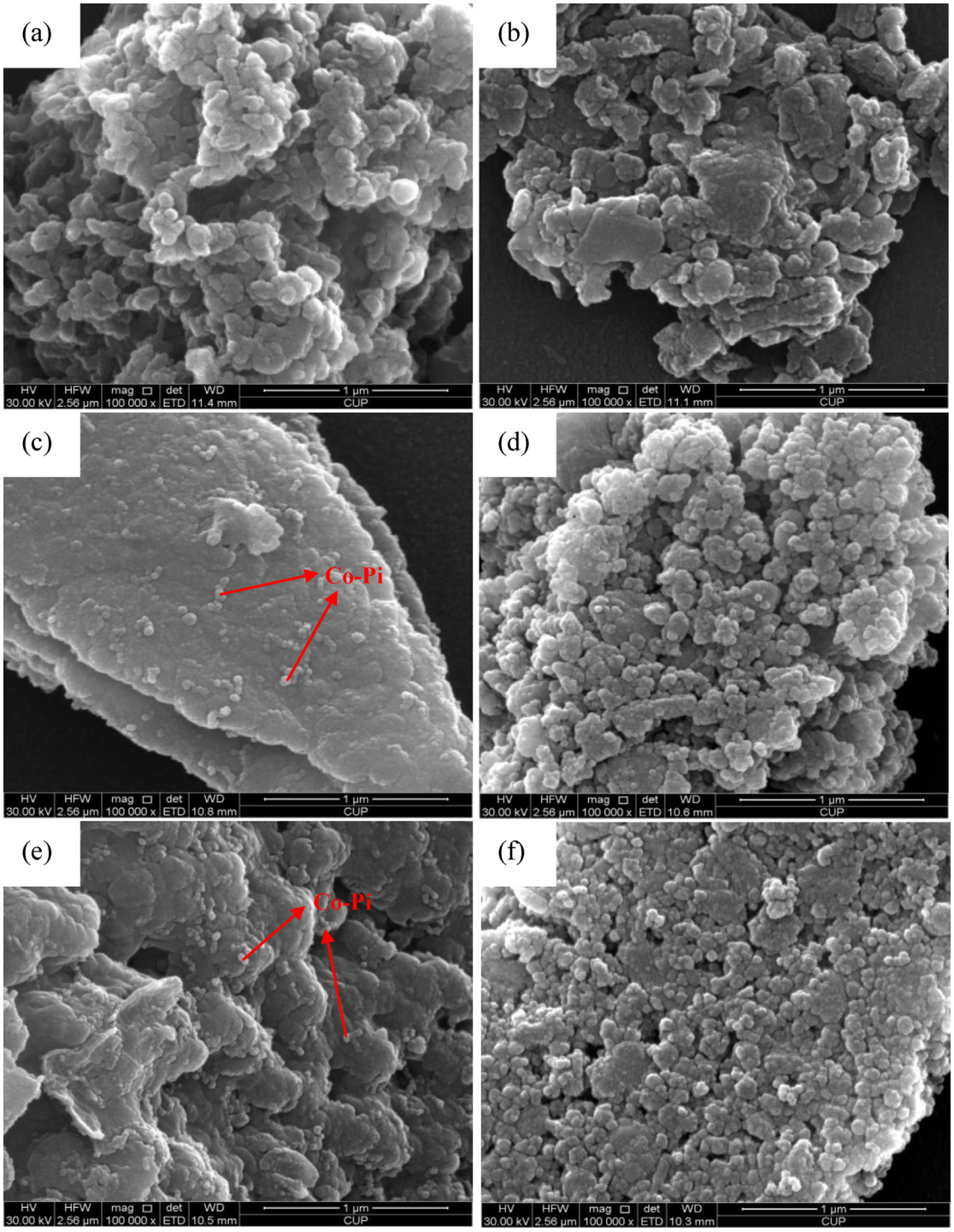

Fig. 2. SEM images of the as-prepared samples: (a) pure g-C_3N_4; (b) CP-5; (c) CP-10; (d) CP-20; (e) CP-30; (f) CP-60.

has two distinct diffraction peaks at 27.5° and 13.2°, which can be indexed for graphitic materials as the (0 0 2) and (1 0 0) peak in JCPDS 87-1526. These two diffraction peaks are in good agreement with the g-C_3N_4 reported in the literatures [8,40]. However, no diffraction peaks corresponding to Co–Pi species can be observed in Fig. 1. The results indicate that the Co–Pi species photochemically deposited on g-C_3N_4 is amorphous and its presence in sample Co–Pi/g-C_3N_4 cannot detected by XRD. This is consistent with the findings reported by other researchers about the formation of the amorphous Co–Pi on various semiconductors [44,49,53,54].

The Co–Pi species was deposited on the g-C_3N_4 surface according to literatures [44,49,51,53] in a 0.1 M potassium phosphate solution (pH = 7) with 0.5 mM cobalt nitrate irradiated with UV light. The oxidation potential of Co^{2+} to Co^{3+} is about 0.7 eV vs. NHE; while the VB edge of polymeric g-C_3N_4 is situated at 1.57 eV vs. NHE. As a result the photogenerated holes have enough overpotential to oxidize Co^{2+} to Co^{3+} to yield the Co–Pi species on the surface of g-C_3N_4 [44]. Fig. 2 illustrates the SEM micrographs of pure g-C_3N_4 and Co–Pi/g-C_3N_4 composite samples with different photochemical deposition time. The pure g-C_3N_4 sample appears to have aggregated microstructures comprising a number of 200–300 nm

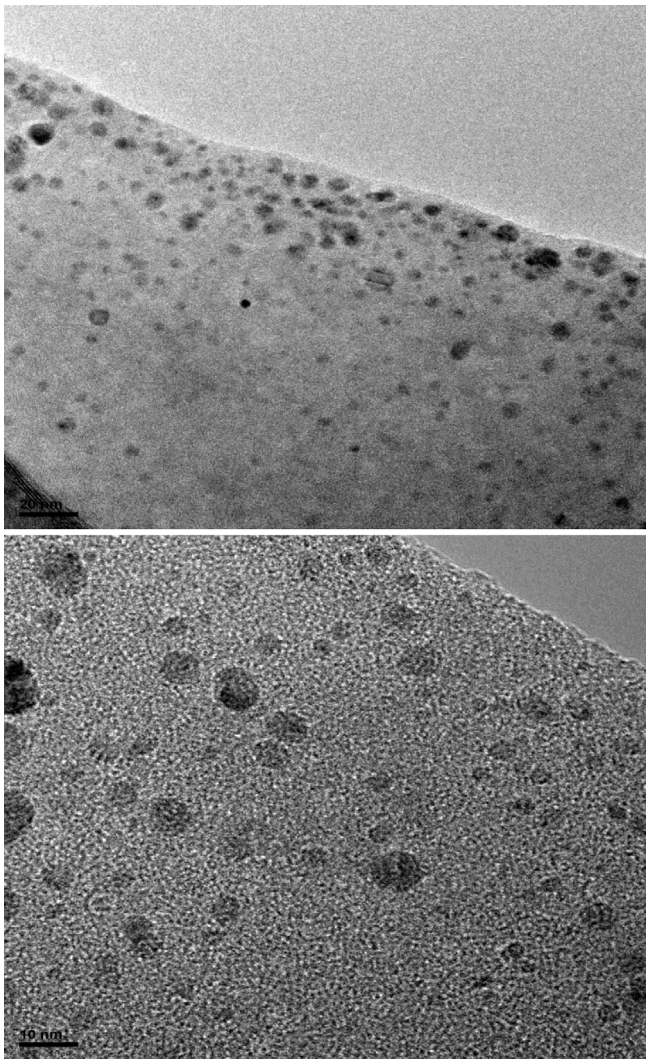

Fig. 3. HRTEM images of Co–Pi/g-C_3N_4 composite photocatalyst (CP-20).

irregular particles. The Co–Pi species are presented as 30–80 nm nanoparticles distributed on the g-C_3N_4 surfaces forming intimate interfaces between Co–Pi and g-C_3N_4 in the hybrid samples. Energy dispersive spectroscopy (EDS) results (Fig. S1) prove that the main compositions of the small nanoparticles are Co–Pi species. And the surface composition of Co–Pi/g-C_3N_4 can be further supported by XPS, as discussed later. More Co–Pi nanoparticles appear on the surfaces of g-C_3N_4 leading to the increased surface coverage with the increase in UV irradiation time. Moreover, the "in situ" photochemical deposition allows the Co–Pi species to be deposited where photogenerated holes are the most readily available. The self-site-selective deposition of Co–Pi species allows the most effective use of Co–Pi in collecting photogenerated holes and promoting electron–hole separation during photocatalytic process.

HRTEM was further used to investigate the microstructures of composite samples. Fig. 3 illustrates HRTEM images with different magnifications for CP-20 sample. After the photochemical deposition of Co–Pi species on g-C_3N_4, the Co–Pi was deposited as nanoparticles on the g-C_3N_4 with high dispersion. The HRTEM results indicate the presence of Co–Pi that forms the intimate interfaces in the composite samples that could favor the charge separation and enhance the photocatalytic efficiency.

The UV–vis diffuse reflectance spectra of as-prepared Co–Pi/g-C_3N_4 composite samples were investigated and shown in Fig. 4. The pure g-C_3N_4 sample shows absorption from the UV through the

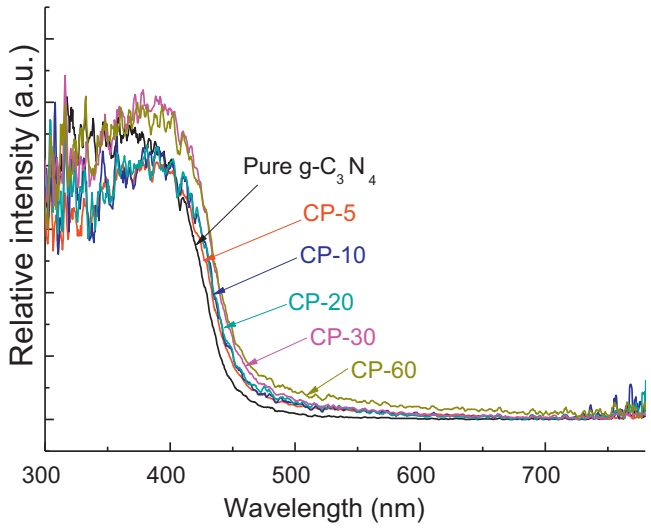

Fig. 4. UV–vis diffuse reflectance spectra of pure g-C_3N_4 and Co–Pi/g-C_3N_4 composite samples.

visible range up to 460 nm. The steep shape of the spectrum indicates that the visible light absorption is ascribed to the band gap transition, corresponding to a band gap of 2.7 eV for g-C_3N_4 [25]. A comparison of the absorption spectra of the pure g-C_3N_4 with the Co–Pi/g-C_3N_4 composite samples shows that the latter exhibit slightly stronger absorption in the visible light region at wavelengths longer than 400 nm, and the red shifts are also observed on the composite samples after "in situ" photodeposition of Co–Pi species. The phenomena may be attributed to the synergistic effect of g-C_3N_4 and Co–Pi co-catalysts in the composite samples. The visible light absorption intensities are also improved with the increase of UV illuminating time for the photodeposition of Co–Pi on the g-C_3N_4 surface and the amounts of Co–Pi deposit (from CP-5 to CP-60). The DRS results also indicate that the photodeposited Co–Pi nanoparticles could enhance the visible light absorption, and hence is expected to increase photocatalytic performance.

The X-ray photoelectron spectrum (XPS) analysis was carried out to gain insight into the chemical composition and binding states on the surface of the Co–Pi/g-C_3N_4 sample. The sample chosen for XPS was CP-20. The XPS spectrum (Fig. S2) shows that the main elements on the surface of the CP-20 are C, N, Co, P and O. The photoelectron peaks appear at binding energies of 288.2 eV (C 1s), 399.1 eV (N 1s), 781.2 (Co 2p), 133.8 (P 2p) and 531.9 eV (O 1s).

Fig. 5 gives the high resolution XPS spectra for CP-20 composite sample in the C 1s (Fig. 5a) and N1s (Fig. 5b) binding energy regions. The C 1s shows two distinct peaks at 284.78 and 288.12 eV, the first peak can be ascribed to carbon species adsorbed on the surface of g-C_3N_4, the second one represents carbon atoms bonding to three nitrogen atoms in the g-C_3N_4 lattice [8,40]. The N1s photoelectron signal can be fitted into three peaks located at 398.44, 399.04 and 400.48 eV, respectively. Two peaks at 399.04 and 400.48 eV can be assigned to tertiary nitrogen (N—$(C)_3$) and amino functional groups having a hydrogen atom (C—N—H) [40,55]. The peak at 398.44 eV is typically attributed to N atoms with sp^2 electrons bonded to two carbon atoms (C=N—C). These spectral data agree well with those reported for g-C_3N_4 [8,40,55].

Fig. 6 illustrates the XPS spectra for the Co 2p and P 2p regions after 20 min photodeposition of Co–Pi to the g-C_3N_4 surface. The split peaks of Co 2p are observed at 781.16 and 797.08 eV, corresponding to Co $2p_{3/2}$ and Co $2p_{1/2}$ orbits respectively (Fig. 6a). The 781.16 eV can be assigned to Co^{2+}, while the other one can be attributed to Co^{3+}. The results agree well with the Co–Pi species reported in the literatures [49,54,56]. The P 2p region shows a

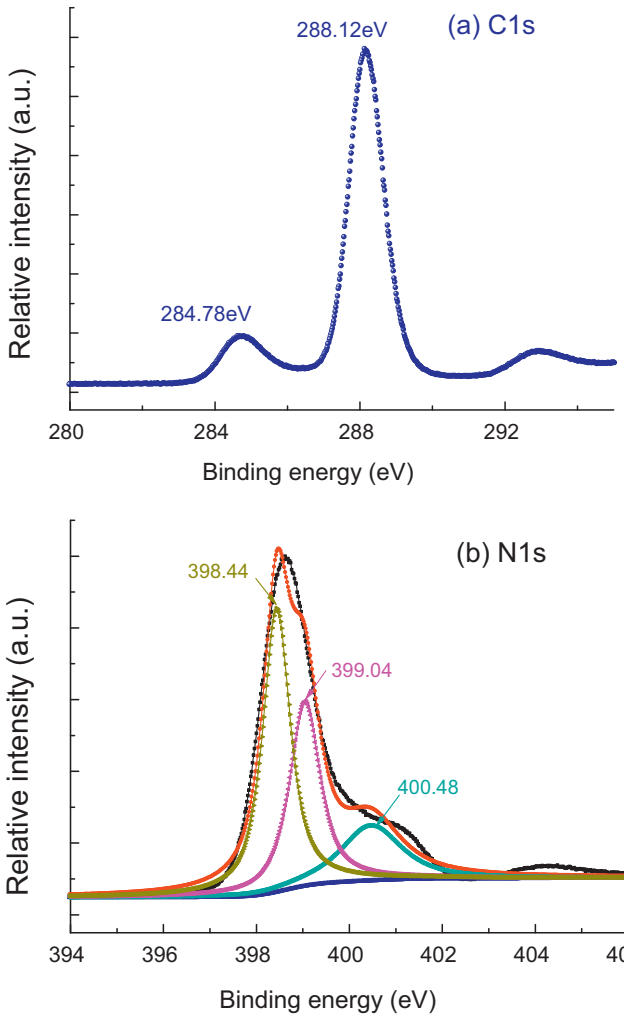

Fig. 5. High-resolution XPS spectra of Co–Pi/g-C_3N_4 composite sample: (a) C1s; (b) N1s.

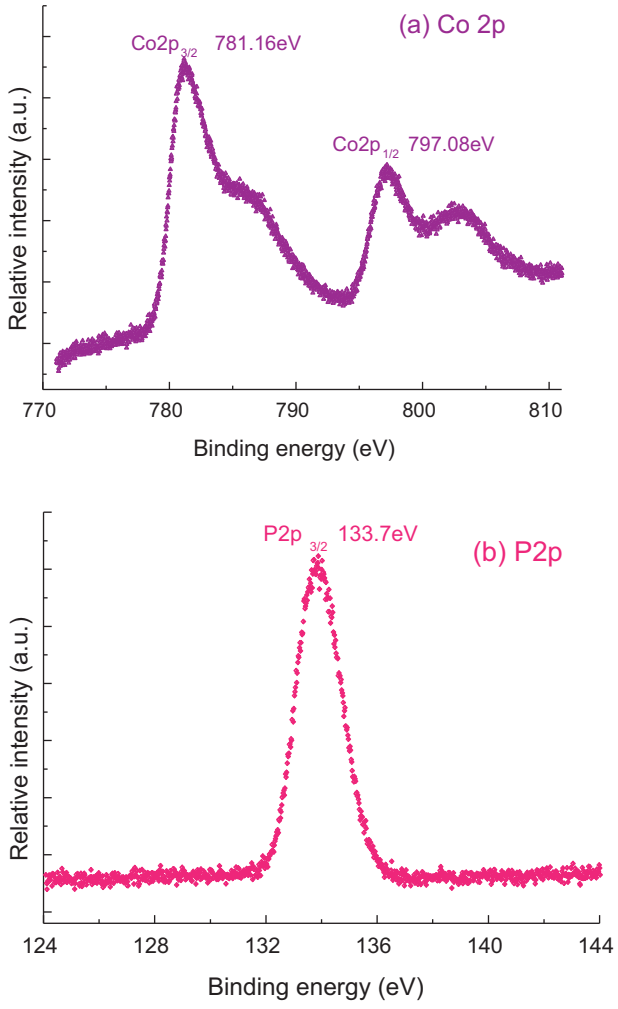

Fig. 6. High-resolution XPS spectra of Co 2p and P 2p of Co–Pi/g-C_3N_4 composite sample.

single peak at 133.7 eV due to phosphate in the Co–Pi co-catalysts [53,54,56]. The existence of Co^{3+} in the sample suggests that Co^{2+} is partially oxidized into Co^{3+} during the photodeposition process. The atomic Co:P ratio in the Co–Pi species is estimated by integrating the Co 2p and P 2p XPS spectra (Table S1), and the results indicate that the atomic ratio of Co:P is 1:0.98. The ratio value is consistent with the number reported in the references [49,53]. Therefore, the XPS results confirmed that the Co–Pi species has been successfully deposited on the g-C_3N_4 photocatalyst in the photodeposition process.

3.2. Photocatalytic performance

The photocatalytic activities of the Co–Pi/g-C_3N_4 composite samples were evaluated by oxygen and hydrogen evolution in aqueous solutions with sacrificial reagents under visible light irradiation (>400 nm). Fig. 7 shows the O_2 evolution curves of Co–Pi/g-C_3N_4 photocatalysts prepared with different photodeposition time, together with the result of pure g-C_3N_4 for comparison using silver nitrate as sacrificial agent. The results demonstrate that the photocatalytic O_2 evolution of pure g-C_3N_4 is very low under visible light irradiation, only 1.28 μmol O_2 is collected after irradiating for 3 h. Wang et al. [54] observed only a trace amount of oxygen generated from pure Co–Pi, indicating that the Co–Pi itself is inactive in oxygen evolution. After photodeposition Co–Pi co-catalyst on g-C_3N_4, the activity of O_2 evolution is enhanced dramatically. The composite sample CP-20 shows the highest O_2 evolving rate. The activity is 6.8 times better than that of pure g-C_3N_4. The amount of Co–Pi is important for the O_2 evolution activity of the composite Co–Pi/g-C_3N_4. In this study, the optimal photodeposition time is 20 min and the CP-20 sample shows the highest O_2 evolution activity.

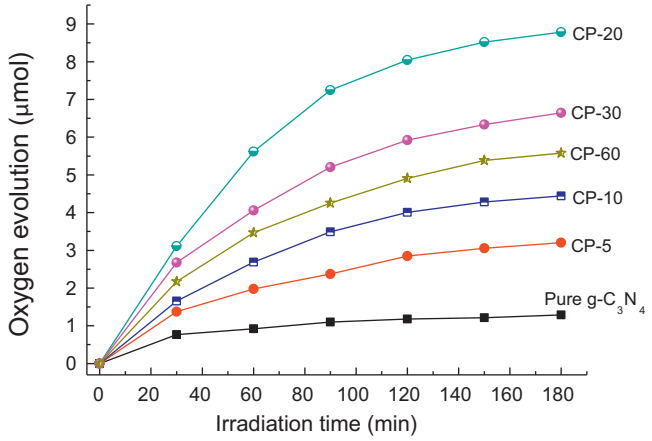

Fig. 7. Photocatalytic O_2 evolution curves of Co–Pi/g-C_3N_4 composite catalysts from 0.02 M silver nitrate aqueous solution under visible light illumination (λ > 400 nm).

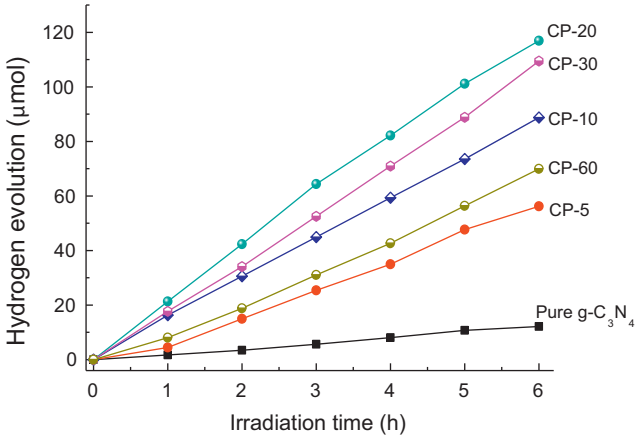

Fig. 8. Photocatalytic H_2 evolution over Co–Pi/g-C_3N_4 composite samples from 25% methanol aqueous solution under visible light illumination ($\lambda > 400$ nm).

The hydrogen evolution over Co–Pi/g-C_3N_4 composite samples was also evaluated in aqueous methanol solution under visible light irradiation, and 1.0 wt% Pt was loaded as a co-catalyst for H_2 evolution. Fig. 8 shows the H_2 production curves for Co–Pi/g-C_3N_4 composite samples. As shown in Fig. 8, pure g-C_3N_4 sample shows visible light photocatalytic activity with H_2 evolution rate of 2.03 μmol h^{-1}. After loading Co–Pi on g-C_3N_4 via photodeposition, H_2 evolution is significantly improved. Similar to O_2 evolution, the H_2 production activity of the composite sample is increased from CP-5 to CP-20. The CP-20 sample shows the highest H_2 evolution rate of 19.48 μmol h^{-1}, which is about 9.6 folds higher than that of pure g-C_3N_4. The results indicate that the loaded Co–Pi can promote separation of photogenerated electron–hole pairs in g-C_3N_4 and enhance the photocatalytic H_2 and O_2 evolution.

In addition to the photocatalytic activity, the stability of a photocatalyst is important in practical applications. In order to study the stability of Co–Pi/g-C_3N_4 catalysts, the cycling hydrogen evolution experiment of CP-20 sample was performed. Fig. 9 shows the H_2 evolution curve in cycling photocatalytic runs. No significant decrease of H_2 evolution is observed after 48 h of irradiation. The XRD analysis (Fig. S3) confirms that the crystal structure of Co–Pi/g-C_3N_4 composite sample (CP-20) does not change after the photocatalytic reaction. The results indicate sufficient stability of Co–Pi/g-C_3N_4 photocatalyst for hydrogen production.

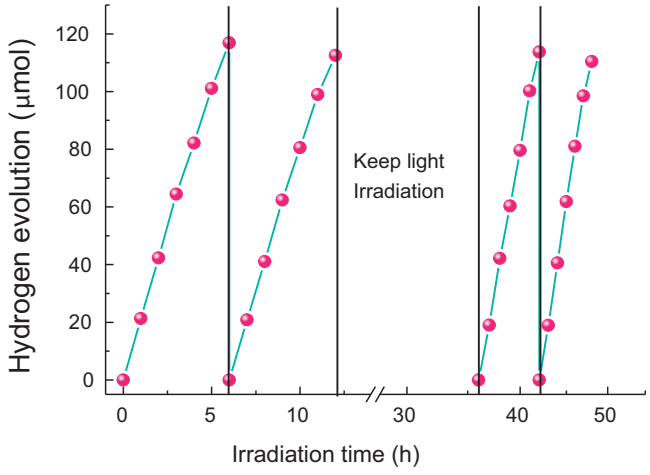

Fig. 9. Cycling runs for the photocatalytic hydrogen evolution in the presence of Co–Pi/g-C_3N_4 (CP-20) composite sample under visible light illumination ($\lambda > 400$ nm).

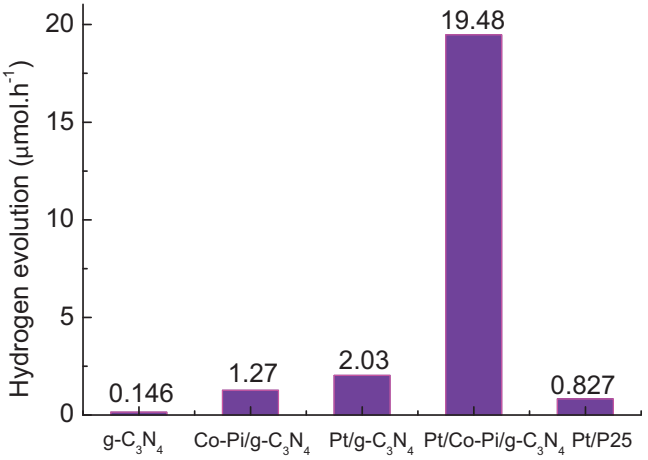

Fig. 10. Comparison of photocatalytic hydrogen evolution on g-C_3N_4 loaded with Co–Pi and Pt, Degussa P25 with 1% Pt from aqueous methanol solution under visible light irradiation.

To further examine the role of Co–Pi in the photocatalytic process, the Pt and Co–Pi were loaded on g-C_3N_4, separately, and their photocatalytic activities were compared. Fig. 10 illustrates the photocatalytic hydrogen evolution of g-C_3N_4 loaded with Co–Pi and Pt, and P25 with 1% Pt loading. The activity of pure g-C_3N_4 without co-catalysts is very low. H_2 evolution is improved upon loading of Co–Pi. The H_2 evolution activity is also increased with the loading 1.0 wt% Pt on g-C_3N_4, indicating that Pt is an efficient co-catalyst for H_2 production. After co-loading the Co–Pi and Pt on g-C_3N_4, the hydrogen evolution is significantly enhanced. The results indicate that the Co–Pi and Pt co-catalyst together can effectively decrease the recombination of electrons and holes in the photocatalytic process. As shown in Fig. 10, the H_2 evolution over Degussa P25 was also carried out as a comparison to the composite photocatalysts [57]. The experimental results reveal that the photocatalytic performance of the Co–Pi/g-C_3N_4 sample is higher than that of P25 photocatalysts under visible light irradiation.

3.3. Photocatalytic mechanism discussion

Based on the results of structure characterization and the visible light photocatalytic activities of the Co–Pi/g-C_3N_4 samples, a possible mechanism is proposed. Fig. 11 shows the "in situ" photodeposition process of Co–Pi on g-C_3N_4. The g-C_3N_4 can be excited under UV light irradiation, and the photogenerated holes have enough overpotential to oxidize Co^{2+} in buffer solution into Co^{3+} ions and form Co–Pi layers with mixed Co^{2+} and Co^{3+} on the g-C_3N_4 surface, whereas the electrons are consumed by the water reduction or react with O_2 in the solution. The Co–Pi nanoparticles are most likely loaded where the holes are generated.

For the photocatalytic process, the efficient charge separation and transfer are crucial for the photocatalytic activity. The Co–Pi species may play a key role in the charge transfer of photogenerated carriers, thus may further contribute to the superior photocatalytic activity of composite samples. As shown in Fig. 12a, for the oxygen evolution reaction, the polymeric semiconductor g-C_3N_4 absorbs photons and excites electron–hole pairs. However, without co-catalysts the photogenerated electrons and holes are likely to recombine, resulting in low photocatalytic activity. The presence of Co–Pi nanoparticles decreases the activation energy of photocatalytic water oxidation. The Co–Pi nanoparticles also serve as the active sites for the oxygen evolution [44,53]. This process also promotes the separation of electron–hole pairs. The electrons reduce the sacrificial reagent Ag^+ into Ag. This electron–hole separation

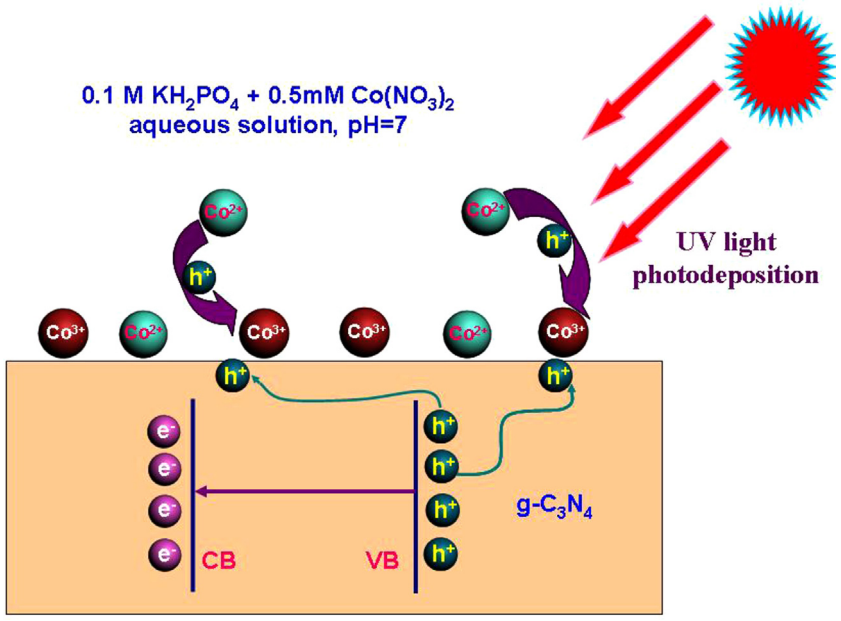

Fig. 11. In situ photochemical deposition of Co–Pi catalyst on the g-C_3N_4 surface.

leads to enhancement of O_2 evolution in the Co–Pi/g-C_3N_4 composite system.

In the photocatalytic hydrogen evolution process as shown in Fig. 12b, both the Co–Pi and Pt are loaded on the g-C_3N_4 surface. The photogenerated electrons could be transferred to Pt and reduce water to form H_2, whereas the holes could be collected by the Co–Pi co-catalyst. And the holes on the Co–Pi surface would prefer to oxidize sacrificial reagent methanol. Therefore, the recombination process of the electron–hole pairs could be partially resulting in the improvement of H_2 production for the Co–Pi/g-C_3N_4 photocatalyst.

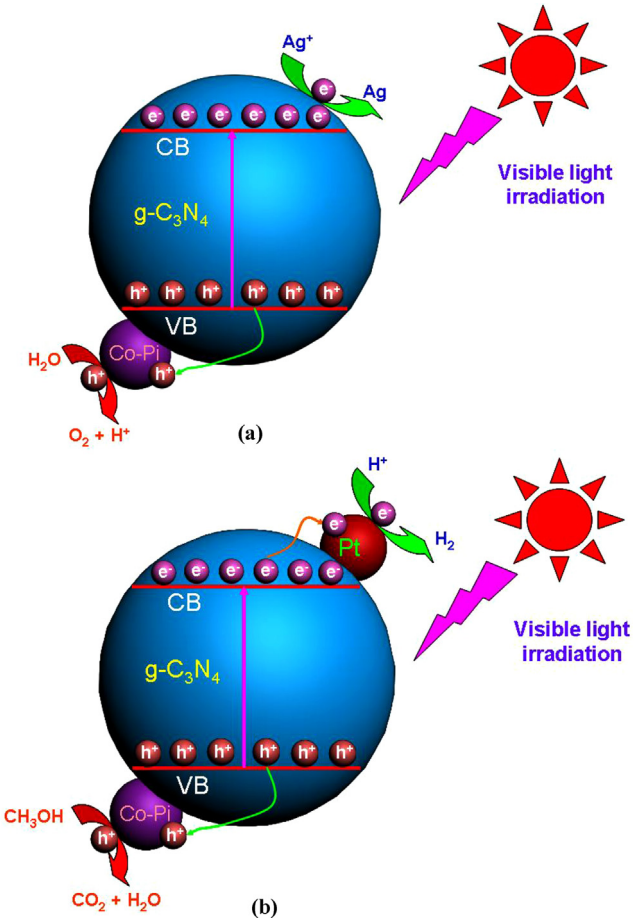

Fig. 12. Proposed photocatalytic mechanisms of Co–Pi/g-C_3N_4 composite system under visible light irradiation: (a) oxygen evolution; (b) hydrogen evolution.

In the present experiment, the CP-20 shows the highest H_2 and O_2 evolution rate, which is about 9.6 and 6.8 times higher than that of pure g-C_3N_4. However, a further increase of photodeposition time can lead to a decrease of water splitting activity. The phenomena can be attributed to loading amount of Co–Pi species. The small amount of Co–Pi may not be sufficient to induce the charge separation. With increasing of UV light irradiation time, more Co–Pi particles are deposited on the surface of g-C_3N_4. The extra Co–Pi particles can shield the active sites on the photocatalyst surface. As a consequence, a suitable content of Co–Pi is crucial for optimizing the photocatalytic performance of Co–Pi/g-C_3N_4 composites.

To further support the proposed photocatalytic mechanism, the photoluminescence emission spectra (PL) and photocurrent curves were performed. Fig. 13 shows the PL spectra for pure g-C_3N_4 and the composite of Co–Pi/g-C_3N_4 samples with an excitation wavelength of 325 nm. The main emission peak centers at about 460 nm for the pure g-C_3N_4 sample, which can be ascribed to the band gap recombination of electron–hole pairs. The emission intensity of PL spectra for the Co–Pi/g-C_3N_4 composites decreases with the increase of photodeposition time. The PL results indicate that the Co–Pi species are effective in the electron–hole pair separation. This could be a reason that the Co–Pi/g-C_3N_4 composites show superior photocatalytic activity under visible light.

The photocurrent of as-prepared samples was investigated with chopped light, which generates both dark current and photocurrent during a single sweep. Fig. 14 presents current–time (I–t) curves of pure g-C_3N_4 and CP-20 electrodes under intermittent visible light irradiation ($\lambda > 420$ nm). Significantly enhanced photocurrent is observed for the Co–Pi photodeposited sample (CP-20) compared to unmodified g-C_3N_4 sample. This suggests that the Co–Pi can enhance the interfacial charge transfer in the composite Co–Pi/g-C_3N_4 sample. The PL spectra and photoelectrochemical (PEC) results support the mechanism discussion above.

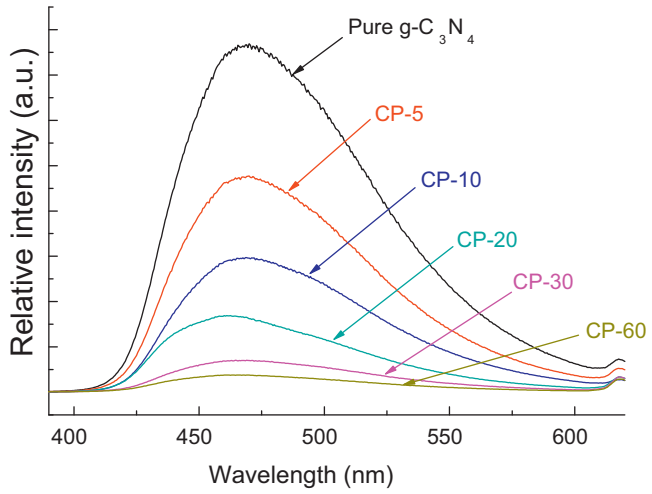

Fig. 13. Comparison of photoluminescence (PL) spectra of pure g-C_3N_4 and Co–Pi/g-C_3N_4 samples.

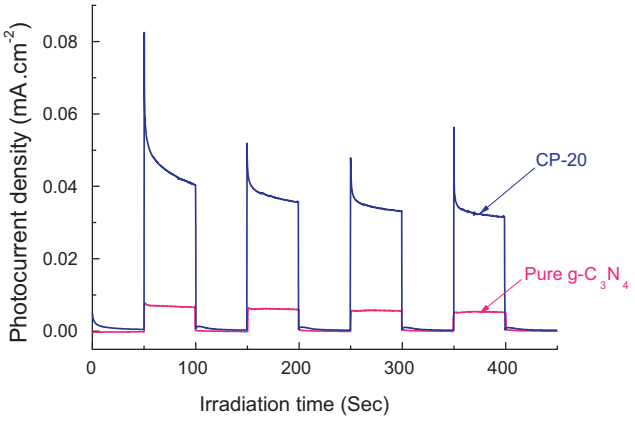

Fig. 14. Transient photocurrent responses (I–t) for pure g-C_3N_4 and CP-20 samples under visible light irradiation at 0.5 V vs. Ag/AgCl.

4. Conclusions

The Co–Pi/g-C_3N_4 composite photocatalysts were synthesized via "in situ" photodeposition method. The Co^{2+} is partially oxidized into Co^{3+} to form Co–Pi species during the deposition process. The Co–Pi species are presented as nanoparticles and distributed on the g-C_3N_4 surface, and the Co–Pi/g-C_3N_4 composites exhibit stronger absorption in the visible light region. The Co–Pi/g-C_3N_4 composite samples show significantly enhanced H_2 and O_2 evolution activities. The CP-20 sample exhibits the highest catalytic efficiency; corresponding O_2 and H_2 evolution are about 6.8 and 9.6 times than those of pure g-C_3N_4. The possible photocatalytic mechanism is proposed; the Co–Pi species can promote the separation of photogenerated charge carriers in g-C_3N_4. The resulting Co–Pi/g-C_3N_4 catalyst constituting of earth abundant elements can be an attractive candidate as high performance photocatalysts for water decomposition.

Conflict of interest

The authors declare no competing financial interest.

Acknowledgements

This work was financially supported by National Science Foundation of China (Grant No. 21003157 and 21273285), Beijing Nova Program (Grant No. 2008B76), and Science Foundation of China University of Petroleum Beijing (Grant No. KYJJ2012-06-20).

Appendix A. Supplementary data

Supplementary data associated with this article can be found, in the online version, at http://dx.doi.org/10.1016/j.apcatb.2013.05.051.

References

[1] X.B. Chen, S.H. Shen, L.J. Guo, A.S. Mao, Chemical Reviews 110 (2010) 6503–6570.
[2] J.G. Yu, G.P. Dai, Q.J. Xiang, M. Jaroniec, Journal of Materials Chemistry 21 (2011) 1049–1057.
[3] L. Ge, M.X. Xu, H.B. Fang, Applied Surface Science 253 (2006) 2257–2263.
[4] X.Q. An, J.C. Yu, Y. Wang, Y.M. Hu, X.L. Yu, G.J. Zhang, Journal of Materials Chemistry 22 (2012) 8525–8532.
[5] S. Linic, P. Christopher, D.B. Ingram, Nature Materials 10 (2011) 911–921.
[6] Y.P. Bi, S.X. Ouyang, N. Umezawa, J.Y. Cao, J.H. Ye, Journal of the American Chemical Society 133 (2011) 6490–6492.
[7] A. Primo, T. Marino, A. Corma, R. Molinart, H. Garca, Journal of the American Chemical Society 133 (2011) 6930–6933.
[8] L. Ge, C.C. Han, Applied Catalysis B: Environmental 117–118 (2012) 268–274.
[9] R. Marschall, A. Mukherji, A.C. Tanksale, H.S. Sun, C.L. Smith, Z. Wang, G.Q. Lu, Journal of Materials Chemistry 21 (2011) 8871–8879.
[10] L. Ge, C.C. Han, J. Liu, Y.F. Li, Applied Catalysis A-General 409–410 (2011) 215–222.
[11] C.C. Lin, T.Y. Wei, K.T. Leea, S.Y. Lu, Journal of Materials Chemistry 21 (2011) 12668–12674.
[12] L. Ge, M.X. Xu, H.B. Fang, Materials Letters 61 (2007) 63–66.
[13] X.B. Chen, L. Liu, P.Y. Yu, S.S. Mao, Science 331 (2011) 746–750.
[14] N. Zhang, S.Q. Liu, X.Z. Fu, Y.J. Xu, Journal of Materials Chemistry 22 (2012) 5042–5052.
[15] A. Iwase, Y.H. Ng, Y. Ishiguro, A. Kudo, R. Amal, Journal of the American Chemical Society 133 (2011) 11054–11057.
[16] S.T. Kochuveedu, D.P. Kim, D.H. Kim, Journal of Physical Chemistry C 116 (2012) 2500–2506.
[17] L. Ge, C.C. Han, J. Liu, Applied Catalysis B: Environmental 108–109 (2011) 100–107.
[18] Q.B. Li, D. Guo, J.G. Yu, J.R. Ran, B.H. Zhang, H.J. Yan, J.R. Gong, Journal of the American Chemical Society 131 (2011) 10878–10884.
[19] Z.G. Yi, J.H. Ye, N. Kikugawa, T. Kako, S.X. Ouyang, H.S. William, H. Yang, J.Y. Cao, W.J. Luo, Z.S. Li, Y. Liu, R.L. Withers, Nature Materials 9 (2010) 559–564.
[20] J.L. Gunjakar, T.W. Kim, H.N. Kim, I.Y. Kim, S.J. Hwang, Journal of the American Chemical Society 133 (2011) 14998–15007.
[21] R. Shi, Y.J. Wang, F. Zhou, Y.F. Zhu, Journal of Materials Chemistry 21 (2011) 6313–6320.
[22] L. Ge, J. Liu, Applied Catalysis B: Environmental 105 (2011) 289–297.
[23] H.N. Kim, T.W. Kim, I.Y. Kim, S.J. Hwang, Advanced Functional Materials 21 (2011) 3111–3118.
[24] Z.H. Li, J.W. Liu, S.J. Wang, Y. Gao, J. Shen, International Journal of Hydrogen Energy 37 (2012) 6431–6437.
[25] X.C. Wang, K. Maeda, A. Thomas, K. Takanabe, G. Xin, J.M. Carlsson, K. Domen, M. Antonietti, Nature Materials 8 (2009) 76–80.
[26] Y. Wang, X.C. Wang, M. Antonietti, Angewandte Chemie International Edition 50 (2011) 2–24.
[27] X.C. Wang, K. Maeda, X.F. Chen, K. Takanabe, K. Domen, Y.D. Hou, X.Z. Fu, M. Antonietti, Journal of the American Chemical Society 131 (2009) 1680–1681.
[28] S.C. Yan, Z.S. Li, Z.G. Zou, Langmuir 25 (2009) 10397–10401.
[29] J.S. Zhang, M. Grzelczak, Y.D. Hou, K. Maeda, K. Domen, X.Z. Fu, M. Antonietti, X.C. Wang, Chemical Science 3 (2012) 443–446.
[30] F. Dong, L.W. Wu, Y.J. Sun, M. Fu, Z.B. Wu, S.C. Lee, Journal of Materials Chemistry 21 (2011) 15171–15174.
[31] Y. Wang, X.C. Wang, M. Antonietti, Y.J. Zhang, ChemSusChem 3 (2010) 435–439.
[32] Y.J. Zhang, T. Mori, L. Niu, J.H. Ye, Energy & Environmental Science 4 (2011) 4517–4521.
[33] F.Z. Su, S.C. Mathew, G.X. Lipner,.Z. Fu, M. Antonietti, Journal of the American Chemical Society 132 (2010) 16299–16301.
[34] X.H. Li, J.S. Zhang, X.F. Chen, A. Fischer, A. Thomas, M. Antonetti, X.C. Wang, Chemistry of Materials 23 (2011) 4344–4348.
[35] X.F. Chen, J.S. Zhang, X.Z. Fu, M. Antonietti, X.C. Wang, Journal of the American Chemical Society 131 (2009) 11658–11659.
[36] G. Liu, P. Niu, C. Sun, S.C. Smith, Z. Chen, G.Q. Lu, H.M. Cheng, Journal of the American Chemical Society 132 (2010) 11642–11648.
[37] S.C. Yan, Z.S. Li, Z.G. Zou, Langmuir 26 (2010) 3894–3901.
[38] Y.J. Zhang, T. Mori, J.H. Ye, M. Antonietti, Journal of the American Chemical Society 132 (2010) 6294–6295.
[39] S.C. Yan, S.B. Lv, Z.S. Li, Z.G. Zou, Dalton Transactions 39 (2010) 1488–1491.
[40] Q.J. Xiang, J.G. Yu, M. Jaroniec, Journal of Physical Chemistry C 115 (2011) 7355–7363.
[41] Y.J. Wang, R. Shi, J. Lin, Y.F. Zhu, Energy & Environmental Science 4 (2011) 2922–2929.

[42] H.J. Yan, H. Yan, Chemical Communications 47 (2011) 4168–4170.
[43] M.W. Kanan, D.G. Nocera, Science 321 (2008) 1072–1075.
[44] E.M.P. Steinmiller, K.S. Choi, Proceedings of the National Academy of Sciences of the United States of America 106 (2009) 20633–20636.
[45] Y. Surendranath, M. Dinca, D.G. Nocera, Journal of the American Chemical Society 131 (2009) 2615–2620.
[46] D.A. Lutterman, Y. Surendranath, D.G. Nocera, Journal of the American Chemical Society 131 (2009) 3838–3839.
[47] Y. Surendranath, D.A. Lutterman, Y. Liu, D.G. Nocera, Journal of the American Chemical Society 134 (2012) 6326–6336.
[48] J.A. Seabold, K.S. Choi, Chemistry of Materials 23 (2011) 1105–1112.
[49] K.J. McDonald, K.S. Choi, Chemistry of Materials 23 (2011) 1686–1693.
[50] J.J.H. Pijpers, M.T. Winkler, Y. Surendranath, T. Buonassisi, D.G. Nocera, Proceedings of the National Academy of Sciences of the United States of America 108 (2011) 10056–10061.
[51] S.K. Pilli, T.E. Furtak, L.D. Brown, T.G. Deutsch, J.A. Turner, A.M. Herring, Energy & Environmental Science 4 (2011) 5028–5034.
[52] D.K. Zhong, S. Choi, D.R. Gamelin, Journal of the American Chemical Society 133 (2011) 18370–18377.
[53] D. Wang, R.G. Li, J. Zhu, J. Shi, J.F. Han, X. Zong, C. Li, Journal of Physical Chemistry C 116 (2012) 5082–5089.
[54] Y.B. Wang, Y.S. Wang, R.R. Jiang, R. Xu, Industrial and Engineering Chemistry Research 51 (2012) 9945–9951.
[55] A. Thomas, A. Fischer, F. Goettmann, M. Antonietti, J.O. Müller, R. Schlogl, J.M. Carlsson, Journal of Materials Chemistry 18 (2008) 4893–4908.
[56] T.H. Jeon, W.Y. Choi, H.W. Park, Physical Chemistry Chemical Physics 13 (2011) 21392–21401.
[57] Y.S. Li, F.L. Jiang, Q. Xiao, R. Li, K. Li, M.F. Zhang, A.Q. Zhang, S.F. Sun, Y. Liu, Applied Catalysis B: Environmental 101 (2010) 118–129.